ACS OMEGA

Article

Cite This: ACS Omega 2018, 3, 529−535

Porous Polymer Bearing Polyphenolic Organic Building Units as a Chemotherapeutic Agent for Cancer Treatment

Piyali Bhanja,[†] Snehasis Mishra,[‡] Krishnendu Manna,[‡] Krishna Das Saha,[‡] and Asim Bhaumik*[,†]

[†]Department of Materials Science, Indian Association for the Cultivation of Science, Jadavpur, Kolkata 700 032, India

[‡]Cancer & Inflammatory Disorder Division, CSIR-Indian Institute of Chemical Biology, Kolkata 700032, India

ABSTRACT: Cancer is one of the most deadly diseases worldwide. Although several chemotherapeutic agents are available at present for its treatment, they have their own limitations. The main problems of these chemotherapeutic agents are cost involvement and severe life-threatening antagonistic effects. Here, we report a new biodegradable N-rich porous organic polymer methylenedianiline-triformyl phloroglucinol (MDTFP-1) synthesized via a Schiff base condensation reaction between two reactive monomers, that is, 4,4′-methylenedianiline and 2,4,6-triformyl phloroglucinol under inert atmosphere. Because this porous polymer contains polyphenolic building units and has a high Brunauer−Emmett−Teller surface area (283 m^2 g^{-1}), it has been explored in the anticancer activity using HCT 116, A549, and MIA PaCa-2 cell lines. We have carried out the flow cytometric assessment using Annexin-V-FITC/PI staining through the exposed level of phosphatidylserine in the outer membrane of cells with MDTFP-1-induced apoptosis. Our results suggested that apoptosis of cells have been enhanced in a time-dependent manner in the presence of this novel porous polymer.

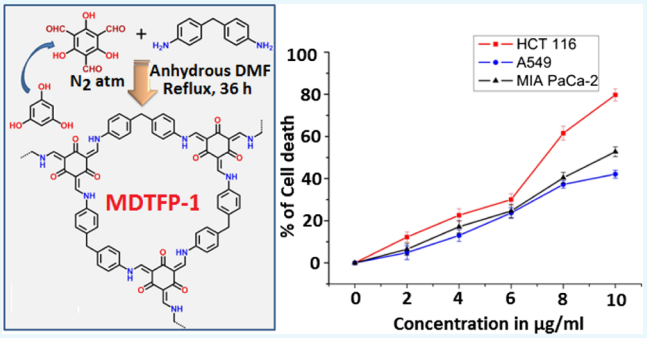

INTRODUCTION

Over the past few decades, cancer has emerged as the major cause of mortality throughout the globe.[1] According to a recent statistics on cancer, 14 million newly diagnosed cases in each year with 8 million mortality and over 32 million people are suffering and undergoing treatment.[2] Lung cancer in male and breast cancer in female population are the leading causes of cancer-related mortality. This exponential rise of cancer is evident owing to the change in human lifestyle, environmental variation, and sun irradiation.[3] The multifactorial environment, genetic basis, and diversity in pathogenesis of different neoplastic etiologies are an obstacle to finding a definitive cure for cancer. The conventional chemotherapeutic agents show a considerable pause in tumor growth and its metastasis, but the serious life-threatening adverse effect (hepatic and renal parenchymal disease and bone narrow aplasia) through destruction of normal cellular homeostasis has been motivating the researchers to find out an alternative way of treatment, which will not only overcome the treatment-related obstacles but also improve the quality of life. Nanomaterials with anticancer activity are intensively studied in the recent times as nanoparticles having a size of less than 100 nm can easily penetrate through the cell and can selectively target the cancer cells without affecting other parts of the body.[4,5] Porous nanomaterials bearing reactive organic moiety in their framework are particularly interesting as they can act as a carrier for drug delivery or itself as an anticancer drug.[6] Apoptosis is an efficient programmed regulation of cellular homeostasis defined by cell biology.[7] Reactive oxygen species (ROS) act as a crucial factor by working as a messenger in a cellular-signaling system to alarm apoptosis.[8] The equilibrium of ROS and the antioxidant is a prime factor, and any alteration of these two causes various cellular harms, leading to inflammatory diseases and carcinogenesis.[9] Thus, induction of apoptosis in cancer cells through the introduction of body-friendly materials can surely open a window from a nanotechnological viewpoint. This aforesaid principle motivated us to explore the anticancer activity of a novel porous nanomaterial bearing reactive organic groups (e.g., polyphenolic compounds) at its surface.

Porous organic polymers (POPs) with tunable nanoarchitecture and functionality can be designed by using a wide range of reactive monomers. A high specific surface area and ease of accommodating reactive functional groups are the most exciting features of these POPs, and these are particularly helpful in exploring their potentials in energy, environmental, and biomedical research.[10] Thus, porous polymers have been utilized in heterogeneous catalysis,[11] gas storage,[12] energy storage,[13,14] sensing,[15] white light emmision,[16] and electrocatalysis.[17] Nanocargos for cancer therapy[18] and imaging[19] are very demanding for the future application of nanomaterials in biomedical research. POPs are largely synthesized through radical polymerization,[20] condensation,[21] cyclization,[22] metal-mediated coupling,[23] and solvothermal[24] condensation reactions. Their huge scope through simple condensation reactions,

Received: October 30, 2017
Accepted: January 2, 2018
Published: January 17, 2018

DOI: 10.1021/acsomega.7b01672
ACS Omega 2018, 3, 529−535

cost-effectiveness, and abundance of C−N bonds in the organic network has motivated the researchers to develop a wide range of POPs. In contrast to metal organic frameworks, zeolites, and metal oxides, the C−N-based organic materials are more environmentally safe and biocompatible. Moreover, the nanoscale porosity, flexible synthesis strategy, diversity in the framework building units as well as the framework stability have made them a promising candidate for biomedical applications.[25]

Although for catalysis, drug delivery, and biomolecule-sensing applications, the porous nanomaterials such as functionalized mesoporous materials,[26,27] covalent organic framework,[28] and graphene-based composites[29] have been utilized, the anticancer activity of the porous polymers bearing organic functionalities is largely unexplored till date. It is noteworthy to mention that curcumin bearing multiple phenolic-OH groups with extended π-conjugation has displayed a remarkable anticancer activity for pancreatic cancer.[30] Herein, we first report the synthesis of a new POP methylenedianiline-triformyl phloroglucinol (MDTFP-1) via a Schiff base condensation reaction between 4,4′-methylenedianiline and 2,4,6-triformyl phloroglucinol. The material has been thoroughly characterized by powder X-ray diffraction (XRD), N_2 sorption analysis, Fourier transform infrared spectroscopy (FTIR), solid-state ^{13}C CP MAS NMR, field-emission electron microscopy (FE-SEM), high-resolution transmission electron microscopy (HR-TEM), thermogravimetric analysis (TGA), and CHN analysis, and its anticancer activity has been explored using various human cell lines.

RESULTS AND DISCUSSION

Nanostructure and Porosity Measurement. The wide-angle powder XRD of the MDTFP-1 material is shown in Figure 1. Here, three broad peaks at a 2θ value of 12.3°, 26.6°, and 43° with low intensities were observed. Thus, these powder XRD data suggested the semicrystalline nature of the polymeric framework. Meanwhile, to determine the porosity of the material in detail, nitrogen adsorption/desorption analysis was performed. The N_2 adsorption/desorption isotherm is shown in Figure 2, where features of both type I and type IV with a small H3 hysteresis loop are observed. In the low pressure region (0.01−0.25 P/P_0), the sharp increase of the adsorption isotherm indicated the presence of microporosity throughout the whole polymer matrix. At a high partial pressure range (P/P_0 = 0.65−0.99), further increase in N_2 uptake suggested the existence of interparticle mesoporosity in the material.[31] The Brunauer−Emmett−Teller (BET) surface area and the pore volume of the material were 283 $m^2\ g^{-1}$ and 0.1633 $cm^3\ g^{-1}$, respectively. The pore size distribution plot has been evaluated by the nonlocal density functional theory (NLDFT) method, where the sharp peak appeared at 1.3 nm, and this is shown in the inset of Figure 2. The De Boer statistical thickness (t-plot) analysis revealed the microporosity and mesoporosity contributions to the total surface area, and these are 240 and 43 $m^2\ g^{-1}$, respectively.

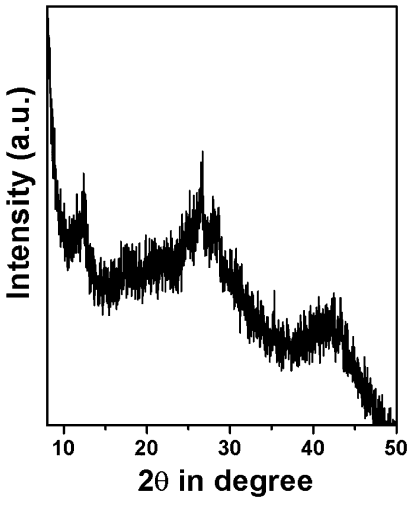

Figure 1. Wide-angle powder XRD pattern of the MDTFP-1 material.

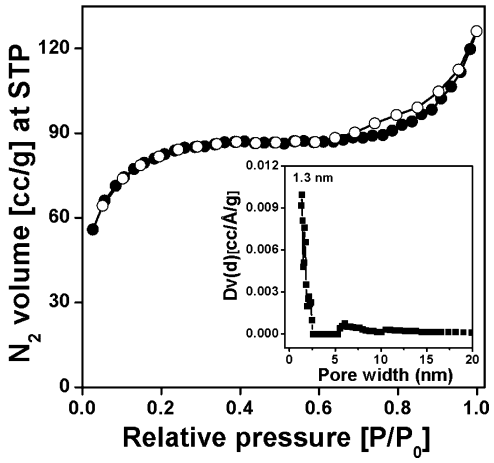

Figure 2. Nitrogen adsorption/desorption isotherm of the MDTFP-1 material, where filled circles represent the adsorption points and empty circles indicate the desorption points. The pore size distribution plot is shown in the inset of the figure.

Spectroscopic Analysis. FTIR spectra of MDTFP-1 and monomers 4,4′-methylenedianiline and triformyl phloroglucinol are shown in Figure 3. One broad and another weak adsorption band were observed at 3425 and 1510 cm^{-1}, respectively. These could be attributed to the −N−H stretching and bending vibrations. The characteristic peak appeared at 1621 cm^{-1} is attributed to the α,β-unsaturated ketone of the enol tautomer in the polymer moiety. Also, the absence of imine (C═N) and hydroxyl (−OH) stretching bands in Figure 3a can confirm that the material framework does not contain

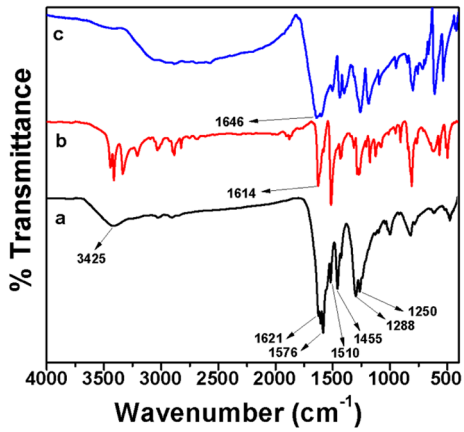

Figure 3. FTIR spectra of MDTFP-1 (a), 4,4′-methylenedianiline (b), and triformyl phloroglucinol (c).

DOI: 10.1021/acsomega.7b01672
ACS Omega 2018, 3, 529−535

any enolic form.[32] The sharp signal appeared at 1576 cm^{-1} suggested the existence of C═Cstretching frequency in the enol to keto tautomerization process. Further, a signal at 1455 cm^{-1} was observed for the −C−H bending vibration, and the strong signal appeared in the vibrational region of 1250−1288 cm^{-1} could be attributed to the formation of the −C−N bond in the polymer matrix. From Figure 3b, the well-defined sharp peaks were noticed at 3420 and 3336 cm^{-1} for the stretching vibration of primary amine groups. For the −N−H in-plane bending vibration, the strong signal was observed at 1614 cm^{-1}. Figure 3c represents the IR spectrum of triformyl phloroglucinol, where the peak was noticed at 1646 cm^{-1} for the carbonyl (C═O) stretching vibration of the aldehyde (CH═O) part in the 1,3,5-triformyl phloroglucinol (TFP) compound.

The solid-state ^{13}C CP MAS NMR spectrum has been recorded to investigate the chemical environment of the MDTFP-1 polymer. Figure 4 represents the solid-state ^{13}C CP MAS NMR spectrum, where the resonance signals are observed at 183, 174, 146, 138, 128, 118, 109, and 100 ppm because of the polymeric framework containing various types of carbon atoms. The strong signal appeared at 183 ppm for the carbonyl carbon atom and along with this, another low intensity peak at 174 ppm was originated because of aromatic ring carbon adjacent to the −N−H groups.[32] Also, the absence of a distinctive peak at 191 ppm confirms all the aldehyde groups of the triformyl phloroglucinol moiety participated in the Schiff base condensation reaction.[33] The resonance signal noticed at 146 ppm was attributed to the formation of enamine carbon.

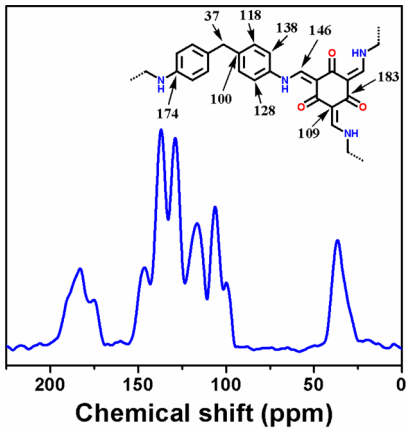

Figure 4. Solid-state ^{13}C CP MAS NMR spectrum of the MDTFP-1 polymer. The model framework with the chemical shifts for different carbon atoms are shown in the inset.

The remaining abovementioned signals, that is, 138, 128, 118, 109, and 100 ppm, are observed for aromatic carbon centers. The characteristic peak at 109 ppm revealed the existence of sp^2 carbons of the phloroglucinol moiety. The sharp peak appeared at 37 ppm could be assigned because of the $-CH_2$ group present in the polymer framework.

Electron Microscopic Analysis. To get an idea about the morphology of the porous polymer, FE-SEM analysis has been carried out. The FE-SEM images of the MDTFP-1 material are shown in Figure 5a,b, where the small rodlike particle morphology with diameter in the range of 30−50 nm was observed. On the other hand, HR-TEM analysis has been carried out to understand the nanostructure of the porous polymer. Figure 6a,b represents the HR-TEM images of the MDTFP-1 material. As noticed from Figure 6a, the pores having a diameter of ca. 1.2 nm are spread throughout the whole specimen, and this confirmed the microporous nature of the material.

Thermal Stability and CHN Analysis. To understand the thermal stability of the MDTFP-1 material, TGA has been performed in the temperature region of 25−800 °C. The first weight loss in the temperature range of 205−315 °C was observed due to the decomposition of organic functional groups, and the second weight loss was observed in the temperature region of 370−600 °C for burning the residual part of the polymer matrix. Figure 7a,b represents the TGA and differential thermal analysis (DTA) profile diagrams of the material, respectively, which suggested that the polymer has considerably good thermal stability. This is essential for carrying out the biomedical application under solvent media. Further, we have carried out CHN elemental analysis of MDTFP-1. The CHN analysis revealed the carbon, hydrogen, and nitrogen contents in the polymer framework as C = 47.23%, H = 5.26%, and N = 8.62% (experimental), respectively. Theoretically, the carbon, hydrogen, and nitrogen contents in the proposed polymeric framework (Scheme 1) are calculated to be C = 46.15%, H = 5.31%, and N = 8.27%, respectively. Good resemblance of the theoretical and experimental composition data suggested nice fitting of the proposed model framework of MDTFP-1.

Anticancer Activity. Our study revealed that MDTFP-1 exhibited appreciable cytotoxicity toward a panel of three cancer cell lines (HCT 116, MIA PaCa-2, and A549 cell line) as per the data of MTT assay. Treatment with different concentrations of MDTFP-1 (0−10 μg/mL) for 24 h amplified the cell death significantly (Figure 8), and the IC_{50} value (5.69 ± 1.02 μg/mL) is lowered toward HCT 116 compared to the other two cell lines. In the case of IC_{50} of the chemotherapeutic

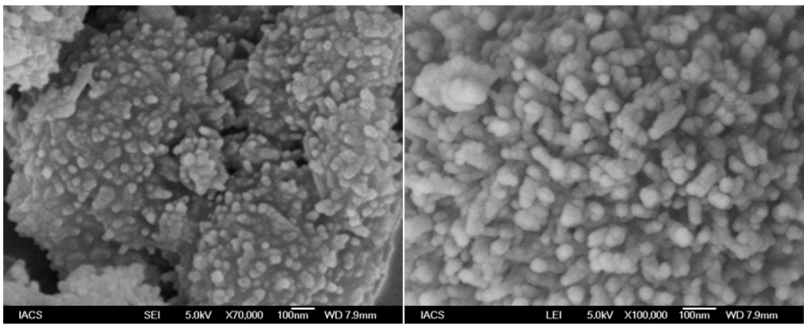

Figure 5. FESEM images of MDTFP-1 at two different magnifications.

DOI: 10.1021/acsomega.7b01672
ACS Omega 2018, 3, 529−535

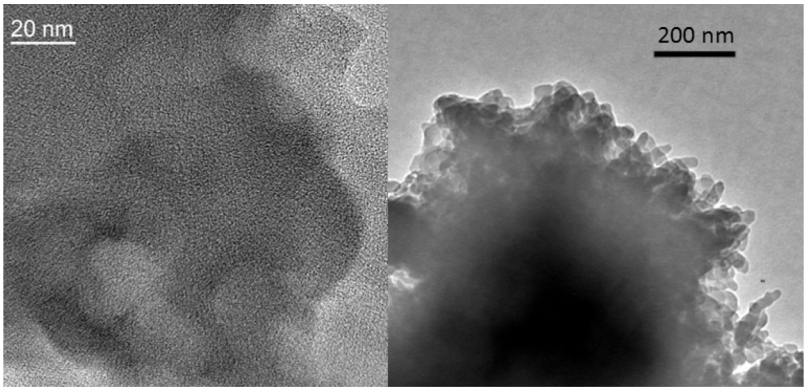

Figure 6. HRTEM images of MDTFP-1 at two different length scales.

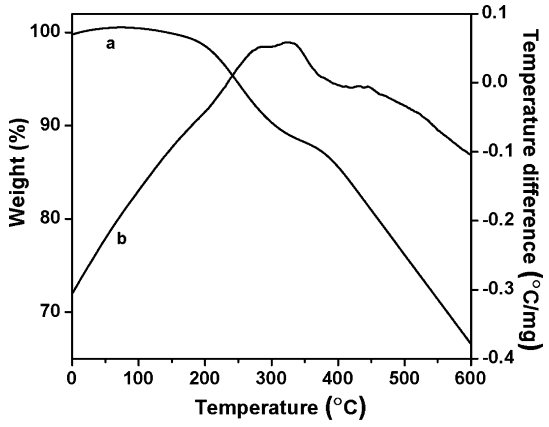

Figure 7. TGA (a) and DTA (b) profiles of the MDTFP-1 material.

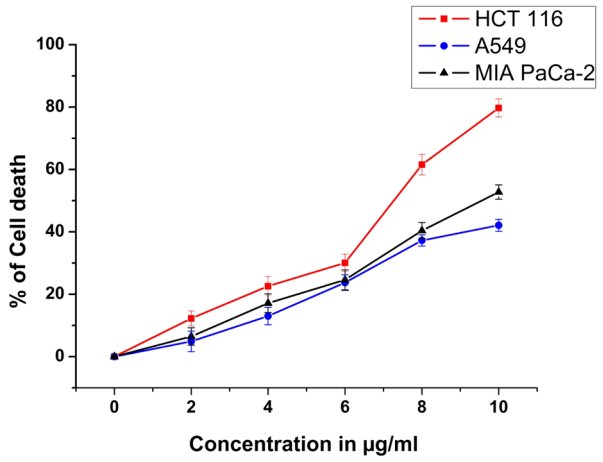

Figure 8. Effect of increasing doses (0–10 μg/mL) of MDTFP-1 on different cancer cell lines in 24 h.

Scheme 1. Schematic Representation for the Synthesis of the MDTFP-1 Porous Polymer

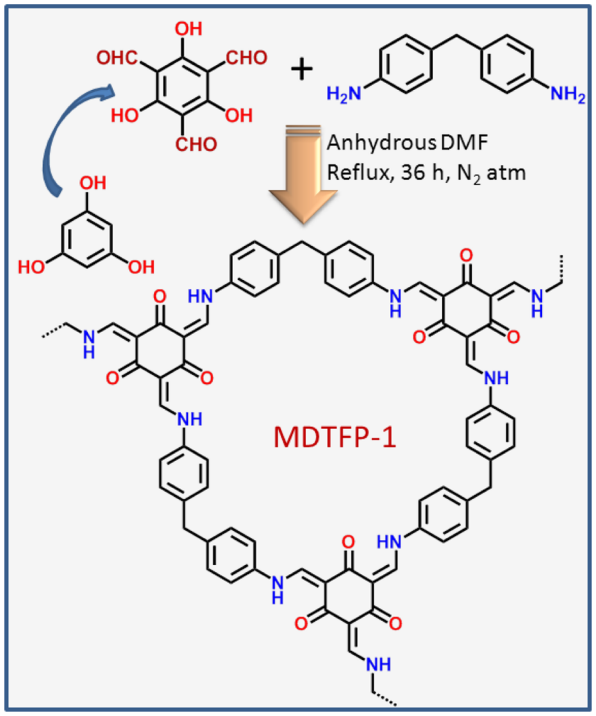

drug, 5-fluorouracil is 10.24 ± 2.14 μg/mL. Therefore, the concentration of 6 μg/mL was selected for the other experimentation by using HCT 116 cells.

Apoptosis is generated by elevated ROS, and thus, we have checked the ROS generation (Figure 9). The mean fluorescence intensity of dihydrodichlorofluorescein (DCF) was significantly (p < 0.05) increased in a time-dependent manner upon MDTFP-1 treatment. We have carried out the experiments multiple times, and the relative DCF fluorescence intensity plots are displayed in a time-dependent manner. To discover whether MDTFP-1 was involved in apoptosis/necrosis, we have carried out the flow cytometric assessment using Annexin-V-FITC/propidium iodide (PI) staining by studying the exposed level of phosphatidylserine in the outer membrane of cells. Our result showed that the % of apoptotic (early and late) cells has been enhanced by a time-dependent manner (6.63% EA/21.5% LA for 6 h, 5.69% EA/26.3% LA for 12 h, and 3.05% EA/19.7% in LA for 24 h) with respect to the control cells (3.08% EA and 9.34% LA) (Figure 10).[34] These results suggested that the MDTFP-1-induced cell death was related to cytotoxicity followed by apoptosis. We have checked this porous polymer MDTFP-1 in the normal cell line HEK293 (human embryonic kidney cells), where we observed that the IC_{50} value is 20 μg/mL, and this is three times more than HCT 116. This result suggested that our MDTFP-1 is highly potential for cancer treatment without affecting the normal tissues.

DOI: 10.1021/acsomega.7b01672
ACS Omega 2018, 3, 529–535

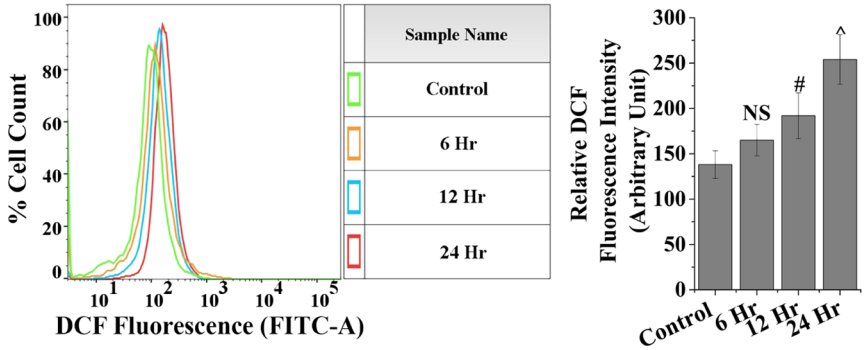

Figure 9. ROS level with time in 6 μg/mL of MDTFP-1 treated HCT 116 cells.

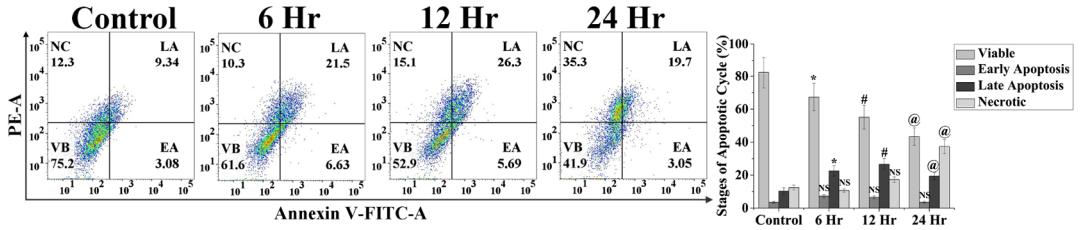

Figure 10. Annexin V, FITC-/PI-positive cells with time of treatment of 6 μg/mL of MDTFP-1 by flow cytometry on HCT 116 in a time-dependent manner.

CONCLUSIONS

Our experimental results suggested that a nitrogen-rich POP bearing multiple phenolic-OH groups can be synthesized through the Schiff base condensation reaction between 4,4′-methylenedianiline and 2,4,6-triformyl phloroglucinol. The material exhibits a good BET surface area and abundance of phenolic-OH groups at its surface, which motivated us to explore its potential in cancer treatment. Our cell-culture experiment suggested that MDTFP-1 is induced by programmed cell death, apoptosis, and externalization of phosphatidylserine, followed by ROS generation. Thus, the POP MDTFP-1 has potential to be utilized as an anticancer agent to overwhelm the epidemiology of cancer in the future.

EXPERIMENTAL SECTION

Materials. Phloroglucinol (M = 126.11 g/mol), 4,4′-methylenedianiline (M = 198.27 g/mol), and hexamine (M = 140.18 g/mol) were obtained from Sigma-Adrich, India. Trifluoroacetic acid (99.5%) was purchased from Alfa Aesar. Anhydrous *N*,*N*-dimethylformamide (DMF) was obtained from Spectrochem, India, and was used without further purification. All other organic substrates and hydrochloric acid (analytical grade) were procured from E-Merck, India.

Characterization Techniques. To record the nitrogen adsorption/desorption isotherms of the POPs, Quantachrome Autosorb 1-C was used, and the samples were activated for 12 h at 120 °C temperature under high vacuum conditions to get rid of any surface-adsorbed moisture or solvent. The BET surface area and NLDFT pore size distribution of MDTFP-1 were estimated by employing N_2 at a 77 K carbon-slit pore model of Autosorb-1 software from the N_2 adsorption/desorption isotherm. The powder XRD patterns of the solid sample were recorded on a Bruker D8 ADVANCE SWAX diffractometer, which was operated at 40 kV voltage and 40 mA current. The instrument has been calibrated with a standard silicon sample by Ni-filtered Cu Kα (λ = 0.15406 nm) radiation. The solid-state ^{13}C CP MAS NMR spectrum of the polymer was obtained on a Bruker ADVANCE 500 MHz NMR spectrometer using a 4 nm MAS probe with a spinning rate of 5000 Hz, with sideband suppression. To record the FT-IR spectrum of the samples, a PerkinElmer Spectrum 100 was used. The UV−visible diffuse reflectance spectrum of the sample was recorded in a UV 2401PC instrument with an integrating sphere attachment, where $BaSO_4$ was used as a background standard. The HR-TEM images of MDTFP-1 were recorded using a JEOL 2010 TEM instrument operated at 200 kV. The sample for TEM analysis was prepared by dropping a sonicated ethanolic suspension of the sample onto the carbon-coated copper grid. To understand the morphology as well as the particle size of the sample, FE-SEM analysis was carried out in a JEOL JEM 6700 electron microscope. TGA/DTA of MDTFP-1 was performed at a temperature ramp of 10 °C/min in a TGA instrument thermal analyzer TA-SDT Q-600 under air flow. A PerkinElmer 2400 Series II CHN analyzer was used for the elemental analysis of the porous polymer MDTFP-1.

Method for the Synthesis of the Porous Polymer (MDTFP-1). TFP was synthesized using phloroglucinol and hexamine by the Duff formylation reaction method.[35] At first, in a 250 mL round-bottom flask containing hexamethylenetetramine (7.4 g, 52.5 mmol), oven-dried phloroglucinol (3 g, 23.8 mmol) and trifluoroacetic acid (45 mL) were added, and the solution mixture was allowed to stir in a preheated oil bath at 100 °C temperature for about 2 h under nitrogen atmosphere. Then, the reaction mixture was subjected to vigorous stirring for 1 h after slow addition of (150 mL) 3 M hydrochloric acid onto it. After completion of the reaction, the resultant solution mixture was filtered through the cold celite bed, and the filtrate was extracted with dichloromethane and sodium sulfate, where the latter was used as the dehydrating agent. The fluffy off-white-colored solid product was collected after solvent evaporation and characterized through ^{1}H and ^{13}C NMR (electrospray ionization).

The porous polymer MDTFP-1 has been synthesized through the Schiff base condensation reaction between the

DOI: 10.1021/acsomega.7b01672
ACS Omega 2018, 3, 529−535

diamine and trialdehyde monomers. In typical synthesis, 2 mmol TFP (420 mg) and 3 mmol 4,4′-methylenedianiline (594 mg) were taken in a 100 mL dry two-neck round-bottom flask containing 20 mL anhydrous DMF. Then, the solution mixture was allowed to reflux for 36 h under inert atmosphere. After completion of the reaction, the brick-red-colored solid product was formed, and it was collected through simple filtration, followed by repeated washing with DMF, absolute ethanol, and acetone step by step to get rid of any unreacted starting compounds. The solid product was dried in air overnight, and it was allowed for Soxhlet extraction using methanol to get a pure solid product. The observed product yield was 88%, and this porous polymer MDTFP-1 was characterized thoroughly.

Cell Lines and Chemicals. Human colorectal carcinoma (HCT 116), human small lung carcinoma (A549), and human pancreatic carcinoma (MIA PaCa-2) cell lines were purchased from the National Centre for Cell Sciences, Pune, India. Cell culture media, viz., Dulbecco's modified Eagle's medium (DMEM), fetal bovine serum (FBS), penicillin−streptomycin−neomycin antibiotic cocktail, ethylenediaminetetraacetic acid (EDTA), and trypsin were procured from Gibco (Grand Island, NY, USA). Additional raw and fine chemicals were procured from Sisco Research Laboratories, India, and Sigma-Aldrich, USA. Antibodies were obtained from Santa Cruz Biotechnology, USA.

Cell Culture. Briefly, human colorectal carcinoma (HCT 116), human small lung carcinoma (A549), and human pancreatic carcinoma (MIA PaCa-2) cells were cultured at 37 °C in a humidified condition under constant 5% CO_2 in DMEM containing 10% FBS with 1% antibiotic cocktail. After 75−80% confluency, cells were seeded with trypsin (0.25%) and EDTA (0.52 mM) in phosphate buffered saline (PBS) and plated at a necessary density to allow them to re-equilibrate before the experimentation.

Cell Viability. For determining the cell viability, MTT [(4,5-dimethyl-thiazol-2-yl)-2,5-diphenyl tetrazolium bromide] assay was performed to initially check the cytotoxic effects of MDTFP-1.[36] A required number of cells (4×10^3 cells/well) were seeded in a 96 well-plate and treated with MDTFP-1 at different concentrations (0, 2, 4, 6, 8, and 10 μg/mL). After treatment, plates were reserved for 24 h at 37 °C in a humidified CO_2-rich condition (5%). After 24 h of the incubation period, cells were thoroughly washed with PBS, and then, MTT solution (4 mg/mL) was added and kept it in an incubator for 4 h. The absorbance of the DMSO-solubilized intracellular formazan salt was recorded at 595 nm using an ELISA reader (EMax, Molecular Device, USA). In all the cases, the MDTFP-1 samples were sonicated before treating in a cell line to get homogenized mixtures. The final reported biological data were represented after repeating the experiments in triplicate.

Assessment of Apoptosis and Necrosis Using Flow Cytometry. The assessment of apoptosis and necrosis was analyzed by flow cytometry using an Annexin-V FITC/PI apoptosis/necrosis detection kit (Calbiochem, CA, USA).[37] The treated cells (1×10^6) were washed and stained with Annexin-V-FITC and PI in accordance with the manufacturer's instructions. The percentages of viable, apoptotic (early and late) along with necrotic cells were quantified by flow cytometry (BD LSRFortessa, San Jose, CA, USA) equipped with FlowJo software.

Assessment of Intracellular ROS. It has been already reported that mitochondrial ROS is one of the key signaling molecules for apoptosis.[38] Therefore, for that, we have quantified the ROS level. To determine the intercellular ROS, we incubated the treated cells with 2′,7′-dichlorofluorescein diacetate of 10 μM at 37 °C for 25 min before the analysis by the flow cytometer (BD LSRFortessa, San Jose, CA, USA) equipped with FlowJo software. The increment of DCF fluorescence is the symbol of generated ROS inside cells, which was signified as mean fluorescence intensity of DCF.

Statistical Analysis. The results are expressed as mean ± SEM. Statistical significance was determined by comparing between various treatment groups and controls using the one-way analysis of variance. Data were considered statistically significant when p values were <0.05.

AUTHOR INFORMATION

Corresponding Author

*E-mail: msab@iacs.res.in (A.B.).

ORCID

Asim Bhaumik: 0000-0002-4907-7418

Author Contributions

The manuscript was written through contributions of all authors. All authors have given approval to the final version of the manuscript.

Notes

The authors declare no competing financial interest.

ACKNOWLEDGMENTS

P.B. thanks to CSIR, New Delhi, for a senior research fellowship. S.M. wishes to thank UGC-DAE for a project fellowship. We are grateful to Tanmoy Dalui and Binayak Pal for their help in instrumentation. A.B. wishes to thank DST, New Delhi, for providing Indo-Egypt international project research grant.

REFERENCES

(1) Rahib, L.; Smith, B. D.; Aizenberg, R.; Rosenzweig, A. B.; Fleshman, J. M.; Matrisian, L. M. Projecting cancer incidence and deaths to 2030: The unexpected burden of thyroid, liver, and pancreas cancers in the United States. *Cancer Res.* **2014**, *74*, 2913−2921.

(2) Robinson, E.; Silverman, B. G.; Keinan-Boker, L. Using Israel's national cancer registry database to track progress in the war against cancer: A challenge for health services. *Isr. Med. Assoc. J.* **2017**, *19*, 221.

(3) Slattery, M. L.; Hines, L. H.; Lundgreen, A.; Baumgartner, K. B.; Wolff, R. K.; Stern, M. C.; John, E. M. Diet and lifestyle factors interact with MAPK genes to influence survival: the Breast Cancer Health Disparities Study. *Canc. Causes Contr.* **2014**, *25*, 1211−1225.

(4) Kemp, J. A.; Shim, M. S.; Heo, C. Y.; Kwon, Y. J. "Combo" nanomedicine: Co-delivery of multi-modal therapeutics for efficient, targeted, and safe cancer therapy. *Adv. Drug Delivery Rev.* **2016**, *98*, 3−18.

(5) Xiao, K.; Luo, J.; Fowler, W. L.; Li, Y.; Lee, J. S.; Xing, L.; Cheng, R. H.; Wang, L.; Lam, K. S. A Self-Assembling Nanoparticle for Paclitaxel Delivery in Ovarian Cancer. *Biomaterials* **2009**, *30*, 6006−6016.

(6) Hu, X.; Liu, S.; Zhou, G.; Huang, Y.; Xie, Z.; Jing, X. Electrospinning of polymeric nanofibers for drug delivery applications. *J. Controlled Release* **2014**, *185*, 12−21.

(7) Sur, S.; Tiwari, V.; Sinha, D.; Kamran, M. Z.; Dubey, K. D.; Kumar, G. S.; Tandon, V. Naphthalenediimide-Linked Bisbenzimidazole Derivatives as Telomeric G-Quadruplex-Stabilizing Ligands with Improved Anticancer Activity. *ACS Omega* **2017**, *2*, 966−980.

(8) Kruiswijk, F.; Labuschagne, C. F.; Vousden, K. H. p53 in Survival, Death and Metabolic Health: A Lifeguard with a Licence to Kill. *Nat. Rev. Mol. Cell Biol.* **2015**, *16*, 393−405.

DOI: 10.1021/acsomega.7b01672
ACS Omega 2018, 3, 529−535

(9) Jiang, L.; Kon, N.; Li, T.; Wang, S.-J.; Su, T.; Hibshoosh, H.; Baer, R.; Gu, W. Ferroptosis as a P53-Mediated Activity During Tumour Suppression. *Nature* **2015**, *520*, 57−62.
(10) Hug, S.; Stegbauer, L.; Oh, H.; Hirscher, M.; Lotsch, B. V. Nitrogen-Rich Covalent Triazine Frameworks as High-Performance Platforms for Selective Carbon Capture and Storage. *Chem. Mater.* **2015**, *27*, 8001−8010.
(11) Mondal, J.; Trinh, Q. T.; Jana, A.; Ng, W. K. H.; Borah, P.; Hirao, H.; Zhao, Y. Size-Dependent Catalytic Activity of Palladium Nanoparticles Fabricated in Porous Organic Polymers for Alkene Hydrogenation at Room Temperature. *ACS Appl. Mater. Interfaces* **2016**, *8*, 15307−15319.
(12) Modak, A.; Bhaumik, A. Porous carbon derived via KOH activation of a hypercrosslinked porous organic polymer for efficient CO_2, CH_4, H_2 adsorptions and high CO_2/N_2 selectivity. *J. Solid State Chem.* **2015**, *232*, 157−162.
(13) Alcaraz-Espinoza, J. J.; De Melo, C. P.; De Oliveira, H. P. Fabrication of Highly Flexible Hierarchical Polypyrrole/Carbon Nanotube on Eggshell Membranes for Supercapacitors. *ACS Omega* **2017**, *2*, 2866−2877.
(14) Bhanja, P.; Bhunia, K.; Das, S. K.; Pradhan, D.; Kimura, R.; Hijikata, Y.; Irle, S.; Bhaumik, A. A New Triazine-Based Covalent Organic Framework for High-Performance Capacitive Energy Storage. *ChemSusChem* **2017**, *10*, 921−929.
(15) Ma, D.; Li, B.; Cui, Z.; Liu, K.; Chen, C.; Li, G.; Hua, J.; Ma, B.; Shi, Z.; Feng, S. Multifunctional Luminescent Porous Organic Polymer for Selectively Detecting Iron Ions and 1,4-Dioxane via Luminescent Turn-off and Turn-on Sensing. *ACS Appl. Mater. Interfaces* **2016**, *8*, 24097−24103.
(16) Pallavi, P.; Bandyopadhyay, S.; Louis, J.; Deshmukh, A.; Patra, A. A Soluble Conjugated Porous Organic Polymer: Efficient White Light Emission in Solution, Nanoparticles, Gel and Transparent Thin Film. *Chem. Commun.* **2017**, *53*, 1257−1260.
(17) Chandra, D.; Jena, B. K.; Raj, C. R.; Bhaumik, A. Functionalized Mesoporous Cross-Linked Polymer as Efficient Host for Loading Gold Nanoparticles and its Electrocatalytic Behavior for Reduction of H_2O_2. *Chem. Mater.* **2007**, *19*, 6290−6296.
(18) Bhunia, S.; Chatterjee, N.; Das, S.; Saha, K. D.; Bhaumik, A. Porous Polyurea Network Showing Aggregation Induced White Light Emission, Applications as Biosensor and Scaffold for Drug Delivery. *ACS Appl. Mater. Interfaces* **2014**, *6*, 22569−22576.
(19) Zheng, X.; Wang, L.; Pei, Q.; He, S.; Liu, S.; Xie, Z. Metal−Organic Framework@Porous Organic Polymer Nanocomposite for Photodynamic Therapy. *Chem. Mater.* **2017**, *29*, 2374−2381.
(20) Bhanja, P.; Gomes, R.; Bhaumik, A. N-rich Porous Organic Polymer with Suitable Donor−Donor−Acceptor Functionality for the Sensing of Nucleic Acid Bases and CO_2 Storage Application. *RSC Adv.* **2015**, *5*, 74916−74923.
(21) Ding, Z.-D.; Zhu, W.; Li, T.; Shen, R.; Li, Y.; Li, Z.; Ren, X.; Gu, Z.-G. A Metalloporphyrin-Based Porous Organic Polymer as an Efficient Catalyst for the Catalytic Oxidation of Olefins and Arylalkanes. *Dalton Trans.* **2017**, *46*, 11372−11379.
(22) İslamoğlu, T.; Rabbani, M. G.; El-Kaderi, H. M. Impact of Post-Synthesis Modification of Nanoporous Organic Frameworks on Small Gas Uptake and Selective CO_2 Capture. *J. Mater. Chem. A* **2013**, *1*, 10259−10266.
(23) Bi, S.; Li, Y.; Wang, L.; Hu, J.; Liu, H. Constructing Diketopyrrolopyrrole-Based Fluorescent Porous Organic Polymer for Chromo Communication via Guest-to-Host Energy Transfer. *J. Phys. Chem. C* **2017**, *121*, 6685−6691.
(24) Dhanalaxmi, K.; Singuru, R.; Mondal, S.; Bai, L.; Reddy, B. M.; Bhaumik, A.; Mondal, J. Magnetic Nanohybrid Decorated Porous Organic Polymer: Synergistic Catalyst for High Performance Levulinic Acid Hydrogenation. *ACS Sustainable Chem. Eng.* **2017**, *5*, 1033−1045.
(25) Hentze, H.-P.; Antonietti, M. Porous Polymers and Resins for Biotechnological and Biomedical Applications. *Rev. Mol. Biotechnol.* **2002**, *90*, 27−53.
(26) Wan, M.; Zhang, J.; Wang, Q.; Zhan, S.; Chen, X.; Mao, C.; Liu, Y.; Shen, J. In Situ Growth of Mesoporous Silica with Drugs on Titanium Surface and Its Biomedical Applications. *ACS Appl. Mater. Interfaces* **2017**, *9*, 18609−18618.
(27) Zhang, F.; Li, J.; Li, X.; Yang, M.; Yang, H.; Zhang, X.-M. In Situ Surface Engineering of Mesoporous Silica Generates Interfacial Activity and Catalytic Acceleration Effect. *ACS Omega* **2016**, *1*, 930−938.
(28) Li, W.; Yang, C.-X.; Yan, X.-P. A Versatile Covalent Organic Framework-Based Platform for Sensing Biomolecules. *Chem. Commun.* **2017**, *53*, 11469−11471.
(29) Jin, L.; Zeng, Z.; Kuddannaya, S.; Wu, D.; Zhang, Y.; Wang, Z. Biocompatible, Free-Standing Film Composed of Bacterial Cellulose Nanofibers−Graphene Composite. *ACS Appl. Mater. Interfaces* **2016**, *8*, 1011−1018.
(30) Bimonte, S.; Barbieri, A.; Leongito, M.; Piccirillo, M.; Giudice, A.; Pivonello, C.; de Angelis, C.; Granata, V.; Palaia, R.; Izzo, F. Curcumin AntiCancer Studies in Pancreatic Cancer. *Nutrients* **2016**, *8*, 433.
(31) Patra, B. C.; Khilari, S.; Satyanarayana, L.; Pradhan, D.; Bhaumik, A. A New Benzimidazole Based Covalent Organic Polymer Having High Energy Storage Capacity. *Chem. Commun.* **2016**, *52*, 7592−7595.
(32) Kandambeth, S.; Shinde, D. B.; Panda, M. K.; Lukose, B.; Heine, T.; Banerjee, R. Enhancement of Chemical Stability and Crystallinity in Porphyrin-Containing Covalent Organic Frameworks by Intramolecular Hydrogen Bonds. *Angew. Chem., Int. Ed.* **2013**, *52*, 13052−13056.
(33) Modak, A.; Mondal, J.; Aswal, V. K.; Bhaumik, A. A New Periodic Mesoporous Organosilica Containing Diimine-Phloroglucinol, Pd(II)-Grafting and its Excellent Catalytic Activity and Trans-Selectivity in C−C Coupling Reactions. *J. Mater. Chem.* **2010**, *20*, 8099−8106.
(34) Mo, R.; Jiang, T.; DiSanto, R.; Tai, W.; Gu, Z. ATP-Triggered Anticancer Drug Delivery. *Nat. Commun.* **2014**, *5*, 3364.
(35) Yelamaggad, C. V.; Achalkumar, A. S.; Rao, D. S. S.; Prasad, S. K. Luminescent, Liquid Crystalline Tris(N-Salicylideneaniline)s: Synthesis and Characterization. *J. Org. Chem.* **2009**, *74*, 3168−3171.
(36) Nandi, R.; Mishra, S.; Maji, T. K.; Manna, K.; Kar, P.; Banerjee, S.; Dutta, S.; Sharma, S. K.; Lemmens, P.; Saha, K. D.; Pal, S. K. A Novel Nanohybrid for Cancer Theranostics: Folate Sensitized Fe_2O_3 Nanoparticles for Colorectal Cancer Diagnosis and Photodynamic Therapy. *J. Mater. Chem. B* **2017**, *5*, 3927−3939.
(37) Dey, S. K.; Bose, D.; Hazra, A.; Naskar, S.; Nandy, A.; Munda, R. N.; Das, S.; Chatterjee, N.; Mondal, N. B.; Banerjee, S.; Saha, K. D. Cytotoxic Activity and Apoptosis-Inducing Potential of Di-Spiropyrrolidino and Di-Spiropyrrolizidino Oxindole Andrographolide Derivatives. *PLoS One* **2013**, *8*, No. e58055.
(38) Um, H.-D. Bcl-2 Family Proteins as Regulators of Cancer Cell Invasion And Metastasis: A Review Focusing on Mitochondrial Respiration and Reactive Oxygen Species. *OncoTargets Ther.* **2016**, *7*, 5193−5203.

DOI: 10.1021/acsomega.7b01672
ACS Omega 2018, 3, 529−535